Estimation of wind soil erosion in a semi-arid region of Mexico

María de Jesús Guevara-Macías[1], Noel Carbajal[1], Luis F. Pineda-Martínez[2]*

[1]Instituto Potosino de Investigación Científica y Tecnológica AC. San Luis Potosi, SL, Mex.

[2]Universidad Autónoma de Zacatecas, Zac., Mex.

Correspondence

Luis F. Pineda-Martinez, UACS, Universidad Autónoma de Zacatecas, Zacatecas, MEX

Email: lpineda@uaz.edu.mx

Running title: Wind Erosion in a semiarid region of Mexico

ABSTRACT

Land degradation is a global problem. One of the main factors of this degradation is intense winds in the world's arid and semi-arid regions. The wind acts on soils without vegetation cover in increasingly large regions. The impact of dust storms is considerable, from massive soil deterioration to health problems. In the arid regions of northern and central Mexico, the problem of changing land use from grasslands and forests to rainfed agriculture has increased notably in recent decades. Recurring dust storms due to winds associated with the passage of cold fronts have become a severe environmental problem. The Weather Research and Forecasting Model (WRF-Chem) was applied to analyze dust storms that occur mainly during the winter. An analysis was performed for wind speed data in the period from October 2005 to April 2018. It revealed that about 20 events per year exceeded a threshold erosion speed of 9 m/s. Fifteen events with the potential to generate dust storms were selected. The total amount of dust emitted was added together, and an average dust storm was calculated. Since the massive land-use change began approximately 50 years ago, a total erosion effect was estimated for this period. The characterization of eight soil samples revealed the texture of fine silty sands with low clay content and low organic content due to the mechanical processes of removing the finest

fraction. Comparison between observed and modeled dust storm events showed good agreement.

Keywords: Wind erosion, dust storms, numerical modeling, soil loss, WRF-Chem

1. Introduction

The world-wide urban expansion and the corresponding demands of food of the growing population have led to a severe land-use change (Foley et al., 2005). In many cases, the change in land use has mainly been in grasslands and forests into rainfed agriculture and only in some cases irrigation system. The Land Use Change (LUC) has occurred mainly in tropical and semiarid regions of the world (Lambin et al., 2003), where the drought phenomenon is most common (Allen, 2009; McLeman et al., 2014). Additionally, many of these regions are also influenced by intense winds during winter. It causes unfavorable conditions to those areas on which strong wind generates a high soil loss. The wind erosion process in the medium and long term leads to the emergence of desert forms as dunes and sandy soils. Wang et al. (2004) document the phenomenon of the formation of desert areas in different parts of the world.

The degradation of the soil in any form is a global problem, and whose immediate consequence is evident in the decrease in the productive capacity of the agricultural soil (Rodríguez Moreno et al., 2017). Wind erosion and soil deterioration are mainly phenomena in arid and semiarid regions (Dong et al., 2000; Prospero et al., 2002). Wind erosion has some impacts, including dust storms, decreased soil productivity, reduced carbon soil absorption, and global climate change (Schoijet, 2005). In China, the land use on rangeland zones in semiarid and arid areas introducing mixed farming-grazing practices resulted in land degradation caused by wind erosion (Wang et al., 2004). In Colorado Plateau in the USA, the vegetation cover changes, mainly in perennial vegetation, accelerated the rates of dust emission caused by wind erosion (Munson et al., 2011). Land-use change interacting with strong wind is one factor that influences the wind erosion process in southern Iran; this process increases with the increase of the agricultural area (Rezaei et al., 2016). The impact of human activities in semiarid environments has reduced productivity and consequently suffered a loss of biodiversity (Reynolds and Stafford Smith, 2002). In northeastern Mexico, another activity that impacts the soil is excessive grazing caused by goats, which produces a decrease in the vegetation cover of the land by reducing the coverage of shrubs that result in land degradation and make it susceptible to processes of desertification (Manzano and Návar, 2000). Based on remote sensing to describe desertification in Mexico's semiarid region, Lira (2004) proposes a desertification model considering three variables and finally

classified into four groups according to the desertification grade. The study concludes that the very high desertification grade is present when vegetation is absent, and highly reflective soil suffers the meteorological phenomena. Although the low desertification grade was associated with areas with emerging agriculture fields, the results correspond to the summer when the high-density vegetation is present (Lira, 2004).

In northern Mexico and the southwestern United States, some studies have been carried out on wind erosion in the region's relevant desert areas, the Altar desert and the Chihuahua desert (Rivera-Rivera et al., 2009 and 2010; Fitzgerald et al., 2013; Pineda-Martínez et al., 2011; Álvarez and Carbajal, 2019). The importance of investigating wind erosion and its relation to soil loss lies in determining the desertification process, in addition to the impact on factors such as deterioration of air quality (Álvarez and Carbajal, 2019), low visibility (Choi and Fernado, 2008), and the effect on radiation budget (Pineda-Martínez et al., 2011). Arid and semiarid regions with low vegetation density, are particularly prone to wind-blown dust (Álvarez and Carbajal, 2019). In central-north Mexico's semiarid region, evidence about land-use changes is mostly in Microphyllous scrub and rangeland areas change into rainfed farming (SEMARNAT, 2013). In the north-central region of Mexico, there was a massive change in land use from pasture and forest to rainfed agriculture in the last five decades. It is necessary to protect ecosystems against possible changes in land use in areas susceptible to deterioration of soil quality, and it is essential to investigate the damage caused by massive land use change. In the southern part of the Chihuahua desert in Mexico, a process of soil deterioration is currently taking place due to the high winds associated with the passage of cold winter fronts that extend through the region. The main objective of this research is to quantify the land degradation due to wind erosion by applying numerical modeling.

2. Materials and Methods

2.1 Study area

The Chihuahua Desert is identified as an important soil dust source (Prospero et al. 2002; Rivera-Rivera et al. 2009). Specifically, the study area is located in a semiarid region in central-northern Mexico in the southernmost part of the Chihuahua desert, predominantly in the state of Zacatecas (Figure 1a) on the central plateau of Mexico. The region is predominantly a semiarid environment crossed by the Tropic of Cancer between the

principal mountain ranges of the Sierra Madre Occidental and Sierra Madre Oriental (Brito-Castillo et al., 2009). Total annual precipitation varies between 500 mm and 200 mm in the southern and northernmost parts of the state. Desert scrubland and semiarid grassland characterize the vegetation of the region predominantly. The main vegetation categories can be assumed as five main ones described by Rivera-Rivera et al. (2009) as bare soils, agricultural lands, shrub/scrub, grassland, and urban areas.

2.2 Data

Meteorological data were obtained from the network of automatic stations (http://www.zacatecas.inifap.gob.mx) and additionally from the International airport of Zacatecas (ZCL) (Figure 1b). A detailed analysis was performed for wind speed data in the period from October 2005 to April 2018. A threshold of 9 ms^{-1} of sustained wind speed data was applied. This threshold velocity is a necessary condition for the dragging of dust that can lead to dust storms formation (Liu et al., 2008; Csavina et al., 2014). Additional data of temperature and relative humidity were also obtained for outputs model validations.

Considering that the wind speed threshold for sediment transport is satisfied in all selected meteorological stations, we select 15 events occurring between 2006 and 2018. The principal aim was to apply the Weather Research and Forecasting Chem (WRF-Chem) to simulate dust storms that occur mainly during the winter (Kumar et al., 2014; Su and Fung, 2015). The model was fed every six hours with data from the National Centers for Environmental Prediction (NCEP) using the Global Forecast System (GFS) with a resolution of 0.5° x 0.5° degrees. The data include surface variables and three-dimensional variables like temperature, water vapor, and vertical wind profiles in 29 pressure levels (1000 – 10 hPa) (Song, 2018). The WRF-Chem configuration included two domains (Fig. 1a). The configuration of the first domain was 120 x 120 points with a grid size of 15 km. The second domain was 176 x 176 points, with a grid space of 3 km. The domains' central coordinates were established at 22.43º N for latitude and 102.65º W, with 29 vertical levels. The physical settings used in the experiments were the WRF Single-moment 3 Class (WSM3) for the microphysics (Hong et al., 2004), the RRTM scheme for longwave radiation (Mlawer et al., 1997), the Dudhia scheme for the shortwave radiation (Dudhia, 1989), the MM5 scheme for the surface layer (Paulson, 1970), Unified Noah for the land-surface model (Mukul Tewari et al., 2004), and YSU for the planet boundary layer (Hong et al., 2006). The dust emission model calculations were performed using an inert

chemical mechanism that considers only dust concentration. Several parameterizations are included in the WRF-Chem to estimate the amounts of dust emission. In this work, Shao's scheme (2004) was used for the friction velocity threshold, the horizontal sand flux, and the vertical dust flux (Kang et al., 2011). Additional data for synoptic charts were generated by using the NCEP NARR database of the NOAA/ESRL Physical Science Division, Boulder, Colorado (available at https://psl.noaa.gov/). Composites were calculated for all events using the climatology of 1981 to 2010 (Mesinger et al., 2006).ç

2.3 Soil Sampling

An essential aspect of this research was to obtain information about soil properties. For this purpose, eight soil samples were collected in areas previously identified as dust emission areas in the simulations. The eight samples of soil was classified by the size system of classification used by the U.S. Department of Agriculture (USDA) (Gee and Or, 2002). The samples were separated using seven sieves with the following size openings: 125 μm, 180 μm, 250 μm, 500 μm, 600 μm, 1 mm, and 2 mm. The soil samples results separated in sizes were plotted to know the size distribution of the soil particles in the study area. These sizes were compared with the particle sizes used by the WRF-Chem.

3. Results

Figure 2 displays the percentages of soil particle size distribution. Sampling sites were selected for a degradation gradient defined by vegetation indices calculated using satellite images (data not shown). The total samples have a low percentage of the fine-sized grain and clay fraction (<180 μm), indicating soils with loss of fine material. Samples 2 and 7 had the highest percentage of fine sizes, and they were collected in bean cultivation plots. Samples 3, 4, and 5 have a higher proportion of sands > 2 mm). In contrast, the smaller proportion of finer dimensions (<125 μm less than 7%). The total samples vary in the following form: a low percentage of sizes between 125 μm and 180 μm and in sizes <500 μm. In contrast, there is a higher percentage in intermediate sizes (<250 μm) indicating a size classifications as poorly graded sand with silt content (Alfaro and Gomes, 2001; Gee and Or, 2002).

The soil texture for the study area was classified as fine silty sands with low clay content and, in general, with low organic content (Gee and Or, 2002). The samples also show high content of silicates and quartz as previously reported for this region (Lee at al., 2009; Rivera-Rivera et al., 2010; Pineda-Martinez et al., 2011). It is relevant to mention that the samples correspond to sites identified as dust emission sources (Pineda-Martínez et al., 2011).

The synoptic conditions that prevail in winter promote an intensification of wind due to the air masses trough (fronts) traveling from high latitudes towards the south. Some authors have documented the influence of cold fronts on the intensification of winds that generates soil erosion phenomena worldwide (Prospero et al., 2002). The impact has been investigated, for example, in The Great Basin in the Salt Lake region in Utah (USA) (Hahnenberger and Nicoll, 2012; Schultz and Steenburgh, 2020). Several investigations showed the effect that large dust storms generate towards the New Mexico region and Northwest Texas in the Dust Blow region (Lee and Gill, 2015; Prospero et al., 2002; Skiles et al., 2018). These systems also generate dust storms from the southwestern USA region and in northwestern and central Mexico (Álvarez et al., 2020; Rivera-Rivera et al., 2009; Rivera-Rivera et al., 2010).

There is a meteorological pattern that defines these phenomena of dust erosion and dispersion (emission). The synoptic meteorological conditions lead to Dust Events Days (DED); for instance, 68% are associated with this cold front synoptic environment (Hahnenberger and Nicoll, 2012). The analysis of data in the northern region of Mexico allowed identifying dust storm events based on the maximum velocity criteria for a specific area where this kind of event has been previously reported in the central highland region (Altiplano) (Pineda-Martinez et al., 2011). Figure 3 shows the synoptic charts for the geopotential height (HGT) at 700 hPa. A recurring pattern of a high-pressure zone is observed at middle levels in the atmosphere, indicating a pressure edge in the cold air mass that drives the front, in all analyzed cases, from the USA-MEX border to central Mexico, i.e., just in the study region. This entire region is then an erodible zone located in the Chihuahua Desert (Rivera-Rivera et al., 2009).

The cyclonic dynamics of the frontal system propagation is a condition of instability that causes an intensification (Schultz, 2005; Schultz and Steenburgh, 2020). This characteristic of frontogenesis is associated with a shift of winds and an intensification of the gusts of wind. The pressure gradient at the 700 mb in northwestern Mexico level drives the movement of cold air. Sometimes the intensification of winds has been observed after the front passage, for example, for the Utah region in the USA (Mallia et al., 2017). In the altiplano (MEX), wind intensification occurs before the air mass passage (Pineda-Martínez et al., 2011). Geostrophic balance controls the dynamics in the first approximation. The dynamics of the front varies depending on the region and the orientation (Schultz, 2005).
In Figure 4, the data shows the compounds for the DED identified as a dust storm event in the study region. Interestingly, the maximum gradient appears just in that transition in advance of the front that coincides with the region of maximum erosion (emission).

Winds vary seasonally in direction and intensity in the region (Figure 5a). During the winter months, the average wind speed is higher than in the summer. The wind direction is predominantly from South-Southwestern in the winter months. Figure 5a shows the average annual wind speed data of the eight automatic weather stations. From December to April, even May, winds speed intensify as a condition generated by the passage of cold air masses from the north, as a condition of the geostrophic balance (Schultz and Schumacher, 1999; Pineda-Martínez and Carbajal, 2009). During winter in the Chihuahuan Desert, the increase in wind speeds is associated with the passage of cold fronts. These months of intense winds are also low or null rainfall in the Chihuahua Desert (Choi and Fernando, 2008). Both conditions cause a more significant impact on the generation of wind erosion, and consequently the degradation of soil (Rivera-Rivera et al., 2009; Lee et al., 2009), but also as a significant factor of emission of particulate matter into the atmosphere as fugitive emissions (Prospero et al., 2002). These emissions generate a deterioration in air quality in cities and the small towns near this emission zone, even in more remote regions (Prospero et al., 2002; Pineda-Martínez et al., 2009; Álvarez and Carbajal, 2019).

Figure 5b shows the number of days where the wind speed exceeds 9m/s, a speed from which there is a high potential for a dust storm event to develop. In Mexico, the National Meteorological Service counted an average of 44 cold fronts events for the winter season, from September to May, from 2001 to 2016 (SMN, 2018). In this research, the data from

automatic stations allowed the identification of 18 potential events as dust emitters for the period 2005-2018.

Figure 6 shows the prevailing weather conditions for the previous day and the day of the dust event (DED) for the emission area. The data correspond to the Zacatecas International Airport (ZCL) located near the simulation domain's central point. We obtain the hourly average of the 15 DED's of parameters of Sea Level Pressure (SLP), temperature, wind, daily maximum wind, and dew point. In all the front passage cases, the main characteristic is that the wind intensifies between 12 and 15 hours of the DED, presenting the maximum peaks in gusts during those hours. These maximums also coincide with a decrease in SLP and Dew Points. There is no marked decrease in temperatures at the front entrance until the cold air mass in the area is established.

4. Discussion

Table 1 shows a summary of the values of each event simulated by WRF. All events correspond to 2006 - 2018 and between December and April when cold fronts activity is maximum. The maximum concentration values correspond to the events between February and April when the wind speed is higher and the relative humidity is the smallest. The wind speed data also indicate that in some years, the events are more intense, and consequently, the values of PM10 increase as in April 2009 and February 2011. There was also one of the most critical droughts in North America (Seager et al., 2014). In contrast, the years with lower concentrations (2006, 2017) are associated with decreased average wind speed.

The impact of dust storms is considerable, causing massive soil deterioration and health problems due to high air dust concentrations. Based on the average maximum concentration of PM10, each event was grouped into four intensity categories: weak, medium, high, and extreme. Although the amount of PM10 is related to the wind intensity, the classification is probably incomplete due to the complexity of the erosion process. Several factors include the specific incidence of the wind (direction and speed) on the agricultural land areas with high erosion potential, the pre-existing humidity in the soil, and in general, the environmental conditions that determine the loss of soil in this semiarid

region. Since this work aims to analyze the loss of soil, the criteria of PM10 issued are established.

The Figure 7 displays each event feature in particular; they revealed defined patterns of the sources and the dust plume. The calculated events reveal that the front (trough) temporality and spatiality define the maximum point of erosion and dispersion. The highest number of cases was in group IV (low) with a maximum emission of 34 μg/m3. In group III, the medium intensity was between 60 and 120 μg/m3. The high-intensity group II had an average concentration between 50 and 150 μg/m3, above the Mexican Standard (75 μg/m3, an average of 24 hours). On February 3, 2011, the only extreme case had a concentration value of more than 350 μg/m3. This case occurred during a period of extraordinary drought that impacted much of Mexico and the southern USA (Seager et al., 2014).

The emission and transport of dust have a considerable variation depending on the emission source points. It is a more complicated matter to define a priori their characteristics due to the landscape heterogeneity. However, there is a very similar plume pattern in all simulated events, i.e., SW-NE plume orientation, coinciding with the dominant and intense winter winds.

Another characteristic of storm events is duration and persistence. In events of higher wind speed, the transport of dust particles will reach a more considerable distance. In some cases, storms generated in central Mexico have been reported that reach the north of Texas in the USA (Lee et al., 2009; Pineda-Martinez et al., 2011). Seasonal wind patterns also have high interannual variability. It indicates that in some years, the emission of dust will be extreme. For instance, on February 3, 2011, an extreme dust storm occurred. Figure 7a reveals that the concentrations reached values of 520 μg/m3. The emission areas are different; in this case, they are displaced to the east, and the substantial emission range reaches an extension of more than 100 km. In adjacent areas, the emission values are of the order of 160 μg/m3.

In the fifteen selected DED's wind rates higher than 9 m/s, the total dust emission varied between 1.2 tons and 937 tons. It means that not all winds higher than the threshold speed caused dust storms; other factors intervene as a previous rain or even the wind direction.

In urban areas close to the study area, air quality data reported during the winter periods exceeded the Mexican standard in maximum values of 24 hours, for several days. During the years 2006, 2007, and 2008, in cities such as Torreon (210 μg/m3), Durango (180 μg/m3), and Zacatecas (200 μg/m3), average monthly values reached values above the Mexican standard between November and March (SEMARNAT, 2018).

High concentrations of dust are mainly associated with the increase in wind intensity associated with the passage of cold fronts annually. It is a fundamental consequence of the massive change in land use from pasture and forest into agriculture. Besides wind erosion, soil deterioration is also caused by the prevailing open-pit mining activity prevailing in the region.

In recent decades this region has undergone a rapid land-use change, mainly from grassland and shrublands to rainfed agriculture. It is relevant to note that agriculture in the semiarid region has been related to areas of the scarcity of water sources, severe soil degradation, and atmospheric pollution by mineral dust, hence the importance of conducting a study on the erosion processes that occur in this area (Wani et al., 2009). In this region, the rainfall is low during the winter, and the vegetation cover is minimal. Consequently, much of the soil is repeatedly exposed to erosion due to strong winds associated with the passage of cold fronts. Wind speeds analysis revealed that the wind records exceed the speed threshold of 9 m/s for erosion or dust removal in up to 20 events per year in meteorological stations located in the region. However, it is necessary to have better certainty about the formation of a dust storm.

Previous studies on this region reported that soil loss by wind erosion was between 35 and 40 tons/ha (Echavarria-Chairez et al., 2009). Pineda-Martinez et al. (2011) estimated a soil loss of about 9162 tons in 12 hours in a dust storm simulation. Since in the study region, reddish soils are dominant, Figure 8 shows a typical reddish dust storm (March 18, 2008). The image reveals the position of large areas of dust emission. It is important to note that not all dust storms are recorded on satellite images, and measurements of PM10 or PM2.5 at weather stations often do not give the true extent of the dust storm. Based on the study of wind speeds in the eight weather stations mentioned above, it is estimated that there are at least nine dust storms per winter.

The potential loss of soil due to wind is a key factor not only in biological degradation processes but also in matters of air quality. The evaluation of the effect of dust storms generated by intense wind speeds is crucial to estimate the potential effect of deterioration on the farmlands of the region. Several experiments were carried out to calculate the dust emitted during each simulated event as a first exercise of potential soil loss through the application of the WRF-Chem model. In each modeled dust storms, the principal aim was to calculate the amount of total mass of dust emitted during the storm at each grid point considered as an area source. The next step was to calculate an average composite of emissions in each grid point during the 15 storms of modeled dust. The composite allows having a first idea of the average magnitude of the erosion process by area sources in the study period. The yearly average composite allows extrapolating for a total of 50 years, from the early 1970s when an intense change in land use occurred due to the agricultural policies implemented in Mexico. Figure 9 displays the calculated total dust emitted by 450 events in 50 years. This calculation shows the potential for soil loss due to wind effects, which coincides with some previous estimations (Echavarria-Chairez et al., 2009).

5. Conclusions

In the north-central part of Mexico, soil erosion occurs due to intense winds associated with the passage of cold fronts. When the winds are very intense, they cause dust storms with concentrations higher than those established by Mexican standards for PM10 and PM2.5. It implies a severe state of environmental pollution. The fundamental cause of this soil degradation is the massive change of land use towards rainfed agriculture. Seasonal wind patterns have high interannual variability; this indicates that the emission of dust could reach extreme conditions in some years. An analysis of thirteen years of wind data was carried out, finding an average of nine cases of strong winds that exceed the speed limit for dust removal. Of these identified cases of a dust storm, fifteen were selected to be modeled. From these fifteen dust storms, an average dust storm was obtained, and. Assuming that the land-use change process is over 50 years old, this average storm was extrapolated to 50 years. In this way, we obtained a first estimate of the spatial distribution of the mass of dust emitted in 50 years. It was found that concentrations in modeled dust storms exceeded Mexican standards; it agrees with observed data that are of the same order of magnitude. The methodology proposed in this work can help investigate further this environmental problem that occurs clearly in the semiarid areas of Mexico.

Conflict of Interest Statement

The authors declare no conflict of interest

References

Alfaro, S. C., Gomes, L. (2001). Modeling mineral aerosol production by wind erosion: Emission intensities and aerosol size distributions in source areas. *J Geophys Res-Atmos, 106-16*, 18075-18084. https://doi.org/10.1029/2000JD900339

Allen, C. D. (2009). Climate-induced forest dieback: an escalating global phenomenon. *Unasylva, 231(232)*, 43-49.

Álvarez, C.A., Carbajal, N. (2019.) Regions of influence and environmental effects of Santa Ana wind event. *Air Qual Atmos Health 12*, 1019–1034. https://doi.org/10.1007/s11869-019-00719-3

Álvarez, C.A.; Carbajal, J.N.; Pineda-Martínez, L.F.; Tuxpan, J.; Flores, D.E. (2020). Dust Deposition on the Gulf of California Caused by Santa Ana Winds. *Atmosphere, 11(3),* 275; https://doi.org/10.3390/atmos11030275

Brito−Castillo, L., Díaz Castro, S. C., Ulloa Herrera, R. S. (2009). Observed tendencies in maximum and minimum temperatures in Zacatecas, Mexico and possible causes. *Int J Climatol,* 292, 211-221. https://doi.org/10.1002/joc.1733

Choi, Y. J., Fernando, H. J. S. (2008). Implementation of a windblown dust parameterization into MODELS-3/CMAQ: Application to episodic PM events in the US/ Mexico border. *Atmos Environ, 4224,* 6039-6046. https://doi.org/10.1016/j.atmosenv.2008.03.038

SMN (Servicio Meteorológico Nacional) 2018. Cold fronts climatology 2001-2016. Retrieved September 17, 2018. Retrieved from:: https://smn.conagua.gob.mx/es/climatologia/pronostico-climatico/frentes-frios

Csavina, J., Field, J., Felix, O., et al., (2014). Effect of wind speed and relative humidity on atmospheric dust concentrations in semi-arid climates. *Sci. Total Environ. 487*, 82-90.https://doi.org/10.1016/j.scitotenv.2014.03.138

Dong, Z., Wang, X., Liu, L., (2000). Wind erosion in semiarid China: an overview. *J. Soil Water Conserv.,* 55, 439– 444.

Dudhia, J. (1989). Numerical study of convection observed during the Winter Monsoon Experiment using a mesoscale two–dimensional model. J. *Atmos. Sci.*,46**,** 3077–3107. *https://doi.org/10.1175/1520-04691989046<3077:NSOCOD>2.0.CO;2*

Echavarría, C.F.G.; Medina–García, G.; Rumayor–Rodríguez, A. F.; Serna–Pérez, A.; Salinas–González, H.; Bustamante–Wilson, J. G. (2009). *Diagnóstico de los recursos naturales para la planeación de la intervención tecnológica y el ordenamiento ecológico*. INIFAP, CIRNOC, Campo Experimental Zacatecas. Libro Técnico Núm. 10. 174 p.

Foley, J. A., DeFries, R., Gregory, A., Barford, C., Gordon, B., Carpenter, S.R., Chapin, F.S., Coe, M.T., Daily, G.C., Gibss, H.K., Helkowski, J.H., Holloway, T., Howard, E.A, Kucharik, C.J., Monfreda, C., Patz, J.A., Prentice, C., Ramakutty, N., Snyder, P.K. (2005). Global Consequences of Land Use. *Science 309.* Pp. 570-574. DOI: 10.1126/science.1111772

Gee, G.W., and D. Or. (2002). Particle-size analysis. p. 255–293. In J.H. Dane and G.C. Topp (ed.) *Methods of soil analysis*. Part. 4. Physical methods. SSSA Book Ser. 5. SSSA, Madison, WI

Lee, J.A. Gill, T.E. (2015) Multiple causes of wind erosion in the Dust Bowl. *Aeolian Res.* 16-36. https://doi.org/10.1016/j.aeolia.2015.09.002

Hahnenberg, M. & Kathleen, N. (2012). Meteorological characteristics of dust storm events in the eastern Great Basin of Utah, U.S.A. *Atmos Environ*. 601-612. doi.org/10.1016/j.atmosenv.2012.06.029

Hong, Song–You, Jimy Dudhia, and Shu–Hua Chen. (2004). A revised approach to ice microphysical processes for the bulk parameterization of clouds and precipitation. *Mon. Wea. Rev.*, 132, 103–120. doi:10.1175/1520-04932004132<0103:ARATIM>2.0.CO;2

Hong, Song–You, Yign Noh, Jimy Dudhia. (2006). A new vertical diffusion package with an explicit treatment of entrainment processes. *Mon. Wea. Rev.*, 134, 2318–2341. doi:10.1175/MWR3199.1

Instituto Nacional de Investigaciones Forestales Agrícolas y Pecuarias INIFAP. 2018. Red de Monitoreo Agroclimático del Estado de Zacatecas. Retrieved from:: http://www.zacatecas.inifap.gob.mx

Kang, J. Y., Yoon, S. C., Shao, Y., Kim, S. W. (2011). Comparison of vertical dust flux by implementing three dust emission schemes in WRF/Chem. J Geophys *Res-Atmos.* 116D9. https://doi.org/10.1029/2010JD014649

Kumar R., M.C. Barth, G.G. Pfister, M. Naja, G.P. Brasseur. (2014). WRF-Chem simulations of typical pre-mosoon dust storm in norther India: influences on aerosol optical properties and radiation budget. *Atmos. Chem. Phys., 14,* 2431–2446. https://doi.org/10.5194/acp-14-2431-2014

Lambin Eric F., Geist, Helmut J. Lepers, Erika. (2003). Dynamics of Land-Use and Land-Cover Change in Tropical Regions. *Annu Rev Env Resour 28:1,* 205-241. https://doi.org/10.1146/annurev.energy.28.050302.105459

Lee, Jeffrey A., Gill, Thomas E., Mulligan, Kevin R., Dominguez Acosta, M., Perez, Adriana E. (2009). Land use/land cover and point sources of the 15 December 2003 dust storm in southwestern North America. *Geomorphology 105.1-2.*18-27. https://doi.org/10.1016/j.geomorph.2007.12.016

Lira, J. (2004). A model of desertification process in a semi-arid environment employing multi-spectral images. In A. Sanfeliu et al. (Eds.), *Progress in pattern recognition, image analysis and applications*. CIARP 2004, Lecture Notes in Computer Science, 3287, 249–258.

Liu, Z.; Liu, D.; Huang, J.; Vaughan, M.; Uno, I.; Sugimoto, N.; Kittaka , C.; Trepte, C.; Wang , Z.; Hostetler, C.; Winker, D. (2008). Airborne dust distributions over the Tibetan Plateau and surrounding areas derived from the first year of CALIPSO lidar observations. *Atmos Chem Phys. 8.* P. 5045–5060. https://doi.org/10.5194/acp-8-5045-2008

Lu, D., Fitzgerald, R., Stockwell, W. R., Reddy, R. S., White, L. (2013). Numerical simulation for a wind dust event in the US/Mexico border region. *Air Qual Atmos Hlth , 62,* 317-331. https://doi.org/10.1007/s11869-012-0174-7

Mallia, D.V., A. Kochanski, D. Wu, C. Pennell, W. Oswald, and J.C. Lin.(2017). Wind-Blown Dust Modeling Using a Backward-Lagrangian Particle Dispersion Model. *J. Appl. Meteor. Climatol., 56,* 2845–2867, https://doi.org/10.1175/JAMC-D-16-0351.1

Manzano, M.G. Návar, J. (2000). Processes of desertification by goats overgrazing in the Tamailipan thornscrub matorral in north-eastern Mexico. *J Arid Land. Vol. 44.* No. 1. Pp. 17-44. https://doi.org/10.1006/jare.1999.0577

McLeman R.A., Dupre J., Berrang Ford L., Ford J., Gajewski K., Marchildon G.(2014). What we learned from the dust bowl: lessons in science, policy, and adaptation. *Popul. Environ., 35,* 417-440, 10.1007/s11111-013-0190-z

Mesinger F, DiMego G, Kalnay E, Mitchell K, Shafran PC, Ebisuzaki W, Jovic D, Woollen J, Rogers E, Berbery EH, et al. (2006). North American regional reanalysis: a long-term, consistent, high-resolution climate dataset for the North American domain, as a major improvement upon the earlier global reanalysis datasets in both resolution and accuracy. *Bull Am Meteorol Soc, 87*:343–360. doi:10.1175/BAMS-87-3-343.

Mlawer, Eli. J., Steven. J. Taubman, Patrick. D. Brown, M. J. Iacono, and S. A. Clough. (1997). Radiative transfer for inhomogeneous atmospheres: RRTM, a validated correlated–k model for the longwave. *J. Geophys. Res., 102,* 16663–16682. https://doi.org/10.1029/97JD00237

Mukul Tewari, N., Tewari, M., Chen, F., Wang, W., Dudhia, J., Le Mone, M.A., Mitchell, K., Ek, M., Gayno, G., Wegiel, J., (2004). Implementation and verification of the unified NOAH land surface model in the WRF model (Formerly Paper Number 17.5). In *Proceedings of the 20th Conference on Weather Analysis and Forecasting/16th Conference on Numerical Weather Prediction, Seattle, WA, USA* (pp. 11-15). https://ams.confex.com/ams/84Annual/techprogram/paper_69061.htm

Munson, S.M., Belnap, J., Okin, G.S. (2011). Responses of wind erosion to climate-induced vegetation changes on the Colorado Plateau. *PNAS. Vol. 108.* No. 10. Pp. 3854 – 3859. https://doi.org/10.1073/pnas.1014947108

Paulson, C. A. (1970). The mathematical representation of wind speed and temperature profiles in the unstable atmospheric surface layer. *J. Appl. Meteor.*, 9, 857–861. *https://doi.org/10.1175/1520-04501970009<0857:TMROWS>2.0.CO;2*

Pineda-Martinez, L. F., and Carbajal, N. (2009). Mesoscale numerical modeling of meteorological events in a strong topographic gradient in the northeastern part of Mexico. *Clim Dyn, 332-3,* 297-312. https://doi.org/10.1007/s00382-009-0549-0

Pineda-Martinez, Luis F., Carbajal, Noel., Campos-Ramos, Arturo A., Noyola-Medrano, Cristina., Aragón-Piña, Antonio. (2011). Numerical research of extreme wind-induced dust transport in a semi-arid human-impacted region of Mexico. *Atmos. Environ. 45,* 4652–4660. https://doi.org/10.1016/j.atmosenv.2011.05.056

Prospero, J.M., Ginoux, P., Torres, O., Nicholson, S.E., Gill, T.E. (2002). Environmental characterization of global sources of atmospheric soil dust identified with the Nimbus 7 Total Ozone Mapping Spectrometer (TOMS) absorbing aerosol product. *Rev. Geophys. 40 (1),* 1002. https://doi.org/10.1029/2000RG000095

Rezaei, M., Sameni, A., Fallah Shamsi, S.R., Bartholomeus, H. (2016.) Remote sensing of land use/cover changes and its effect on wind erosion potential in southern Iran. *PeerJ 4,* e1948. https://doi.org/10.7717/peerj.1948.

Rivera Rivera, N.I., Gill, T.E., Gebhart, K.A., Hand, J.L., Bleiweiss, M.P., Fitzgerald, R.M., (2009). Wind modeling of Chihuahuan Desert dust outbreaks. *Atmos Environ 43,* 347e354. https://doi:10.1016/j.atmosenv.2008.09.069.

Rivera Rivera, N.I., Gill, T.E., Bleiweiss, M.P., Hand, J.L., (2010). Source characteristics of hazardous Chihuahuan Desert dust outbreaks. *Atmos. Environ. 44,* 2457–2468. http://dx.doi.org/10.1016/j.atmosenv.2010.03.019

Rodríguez, V. M., Ruíz, J., Medina, G., Valenzuela, C., Ruvalcaba, J. y Álvarez, A., (2017). Cambios esperados al uso del suelo en México, según escenario de cambio climático A1F1. *Revista Mexicana de Ciencias Agrícolas. 19,* 3979-3992. http://dx.doi.org/10.29312/remexca.v0i19.667

Seager, R., Goddard, L., Nakamura, J., Henderson, N., Lee, D. E. (2014). Dynamical causes of the 2010/11 Texas–northern Mexico drought. *J. Hydrometeorol. 15(1),* 39–68. doi:10.1175/JHM-D-13-024.1.

SEMARNAT (Secretaría de Medio Ambiente y Recursos Naturales) (2013). *Programa Anual de trabajo de Zacatecas PAT. Secretaría de Agua y Medio Ambiente.* Gobierno del Estado de Zacatecas.

SEMARNAT (Secretaria de Medio Ambiente y Recursos Naturales) (2018). Programa para Mejorar la Calidad del Aire en la Región de la Comarca Lagunera 2010-2015. Retrieved from: : http://www.semarnat.gob.mx/

Schoijet M., (2005). Desertificación y tormentas de arena. (Desertification and sand storms). *Región y Sociedad XVII 32:*167–187

Schultz, D. M., and P. N. Schumacher, (1999). The use and misuse of conditional symmetric instability. *Mon. Wea. Rev., 127,* 2709–2732. https://doi.org/10.1175/1520-04931999127<2709:TUAMOC>2.0.CO;2

Schultz, D. M., (2005). A review of cold fronts with prefrontal troughs and wind shifts. *Mon. Wea. Rev., 133,* 2449–2472, https://doi.org/10.1175/MWR2987.1.

Schultz, D.M. and W.J. Steenburgh, (2020). Nonclassic Evolution of a Cold-Frontal System across the Western United States during the Intermountain Precipitation Experiment IPEX. *Wea. Forecasting, 35,* 255–271, doi.org/10.1175/WAF-D-19-0166.1

Shao, Y. (2004). Simplification of a dust emission scheme and comparison with data *J. Geophys. Res., 109,* doi:10.1029/2003JD004372.

Skiles, S. M., Flanner, M., Cook, J. M., Dumont, M., Painter, T. H., (2018). Radiative forcing by light729 absorbing particles in snow. *Nat Clim Change, 8,* 964-971. https://doi.org/10.1038/s41558-730 018-0296-5

Song, H. and Sohn, B. (2018). An Evaluation of WRF Microphysics for Simulating the Warm-Type Heavy Rain over Korean Peninsula. Asian Pacific. *J Atmos Sci.*, *54(2),* 225–236. https://doi.org/10.1007/s13143-018-0006-2

Stafford Smith DM, Reynolds JF. (2002). Desertification: A new paradigm for an old problem. In Global Desertification: Do Humans Cause Deserts? Reynolds JF, Stafford Smith DM (eds). *Dahlem Workshop Report 88*. Dahlem University Press: Berlin, 403–424 http://hdl.handle.net/102.100.100/200112?index=1

Su, L., Fung, J.C., (2015). Sensitivities of WRF-Chem to dust emission schemes and land surface properties in simulating dust cycles during springtime over East Asia. *J. Geophys. Res. Atmos. 120(11),* 215-11,230. https://doi:10.1002/2015JD023446

Wang, T., Wu, W., Chen, G.T., Xue, X., Sun, Q.W. (2004). Study of spatial distribution of sandy desertification in North China in recent 10 years. *Sci. China Ser. D Earth Sci. 47 (z1),* 78–88. https://doi.org/10.1360/04zd0009

Wang X, Dong Z, Zhang J, Liu L. (2004). Modern dust storms in China: an overview. *J Arid Environ. 58,* 559–574. https://doi.org/10.1016/j.jaridenv.2003.11.009

Wani SP, Sreedevi TK, Rockstrom J, Ramakrishna Y. S., (2009). Rainfed Agriculture – Past Trends and Future Prospects, In: Wani SP, Rockstrom J and Oweis T (eds) (2009). *Rainfed Agriculture: unlocking the potential, Oxfordshire*: CABI International.

Table 1.

Summary of dust events simulated applying the WRF-Chem model. The data correspond to the central point of the D1 in WRF-Chem and the observation data from the meteorological station of Zacatecas International Airport (ZCL). Temperature and relative humidity (RH %) are the 24hour averages for the day of the event. Wind represents de maximum value reached during the DED.

Date of DED	Temperature (°C)		RH (%)		Max Wind (m/s)	
	WRF	ZCL	WRF	ZCL	WRF	ZCL
Dec 29, 2006	5.0	9.9	40.8	43.5	15.8	15.6
Jan 31, 2007	10.3	9.5	59.6	55.3	18.2	12.8
Feb 14, 2007	12.0	13.9	26.5	24.5	14.3	13.9
Feb 16, 2008	13.9	13.9	30.7	25.8	12.3	12.8
Apr 11, 2009	16.9	18.6	25.1	21.8	17.0	15.6
Dec 01, 2009	9.1	10.5	53.9	68.0	19.7	18.1
Mar 09, 2010	11.6	15.1	24.6	43.0	17.4	15.6
Feb 3, 2011	9.9	12.6	64.1	40.9	17.8	17.5
Mar 20, 2012	11.8	14.3	32.7	32.5	12.5	14.4
Feb 21, 2013	12.4	15.2	39.2	30.3	12.4	15.6
Dec 27, 2015	10.1	12.0	48.6	48.7	17.9	18.1
Mar 9, 2016	10.5	7.1	49.0	55.7	18.2	18.1
Feb 13, 2017	14.1	17.1	30.6	25.8	10.9	12.8
Dec 7, 2017	9.1	15.1	46.5	40.0	12.2	18.1
Apr 10, 2018	16.2	17.9	38.8	26.3	30.8	18.1

Figures

Fig. 1

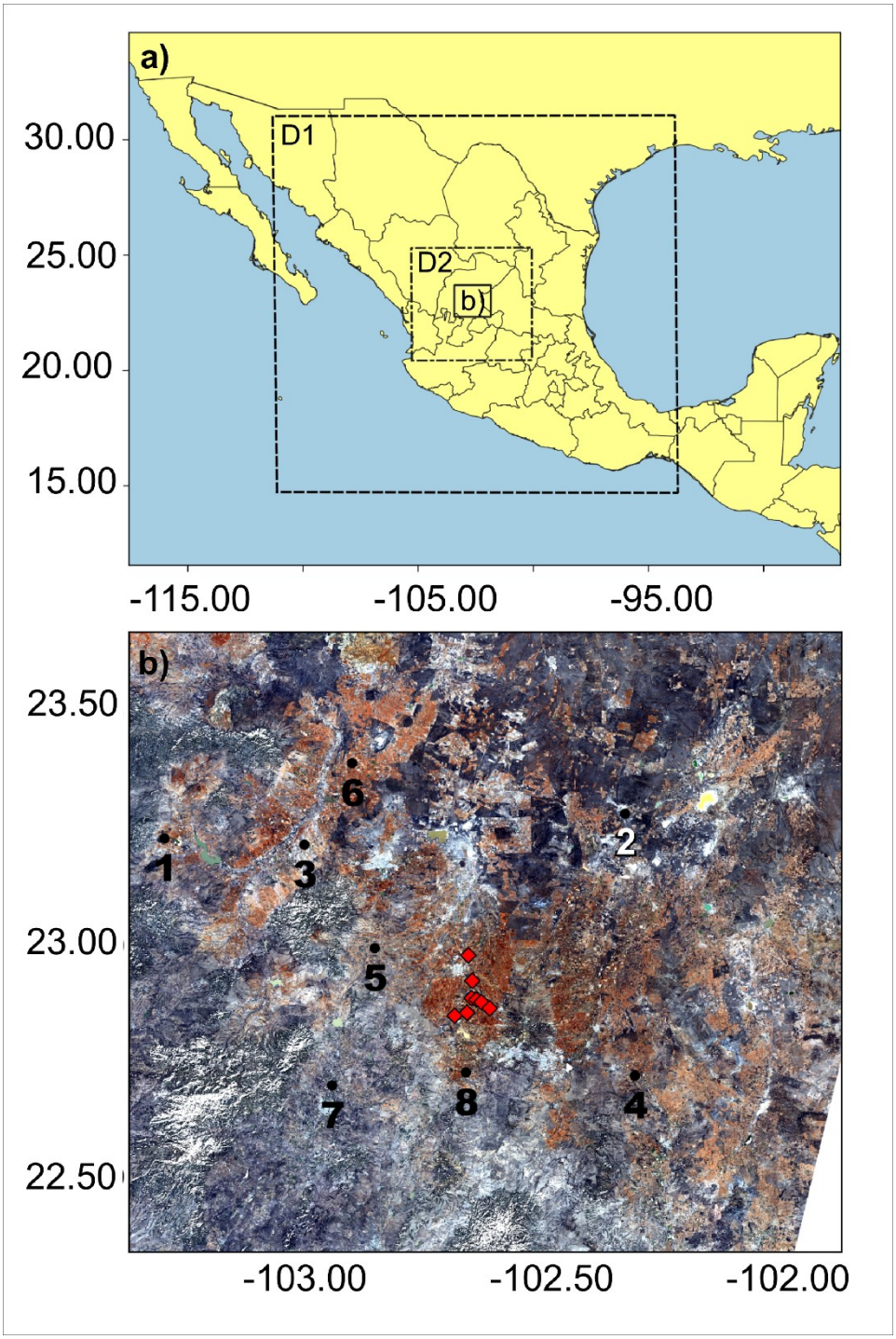

Figure 2

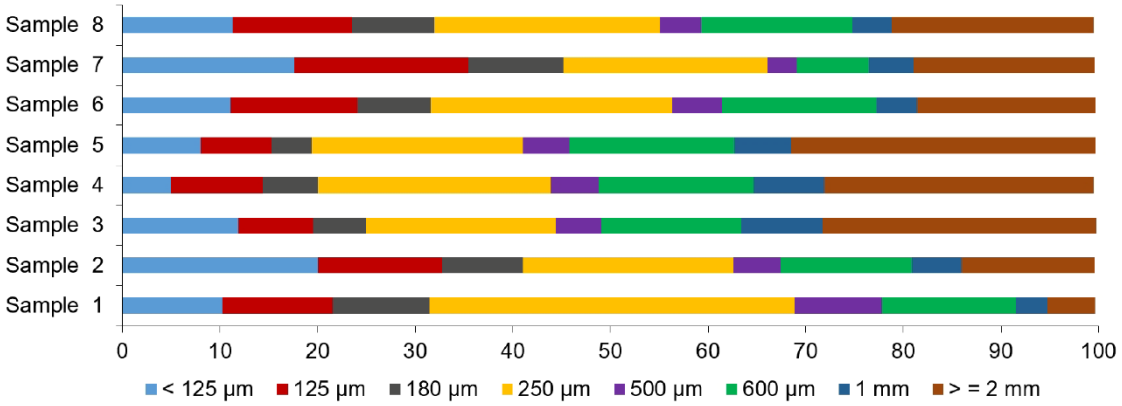
Sample 8
Sample 7
Sample 6
Sample 5
Sample 4
Sample 3
Sample 2
Sample 1
0
10
20
30
40
50
60
70
80
90
100
< 125 µm
125 µm
180 µm
250 µm
500 µm
600 µm
1 mm
> = 2 mm

Figure 3

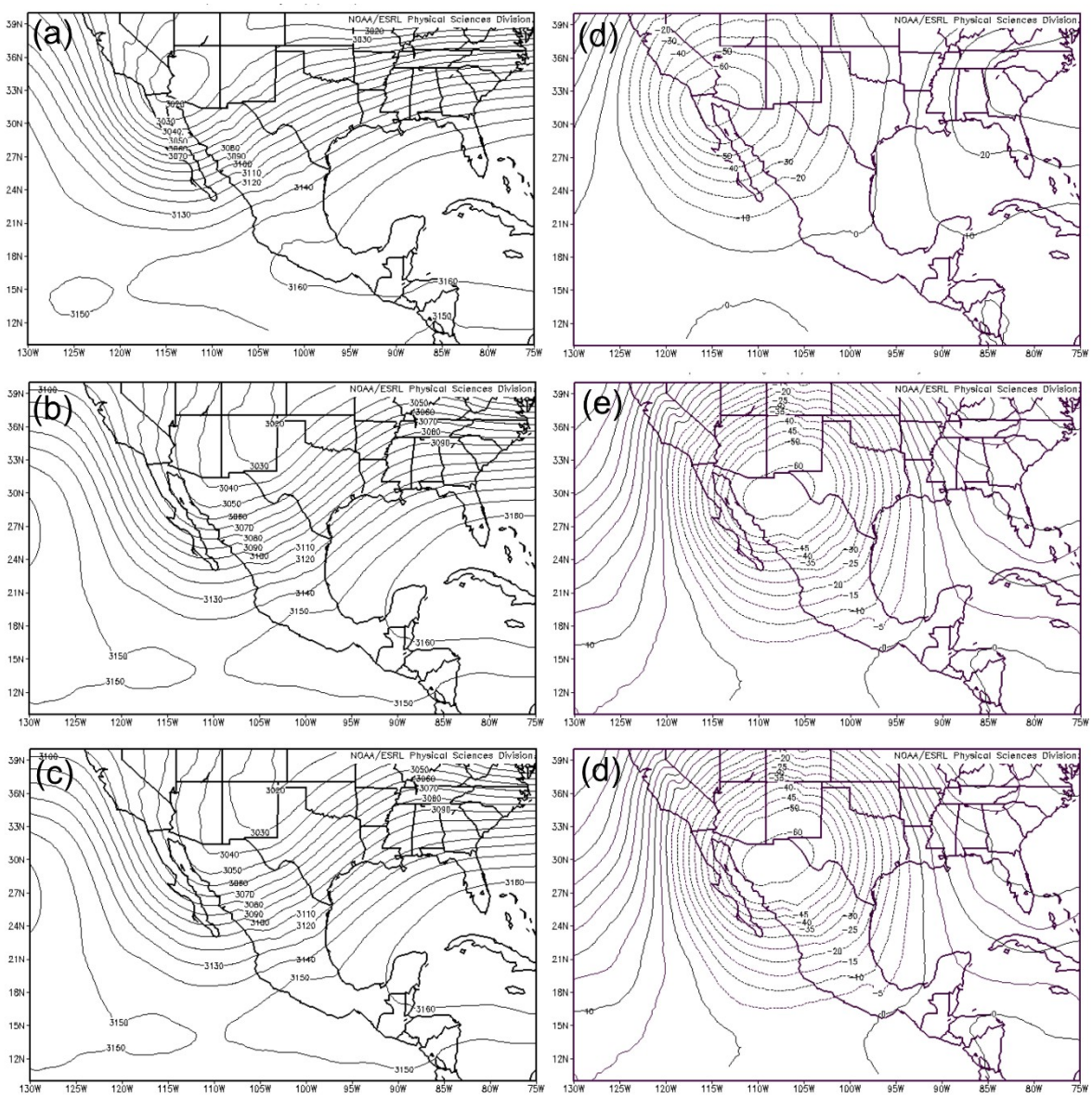

Fig 4

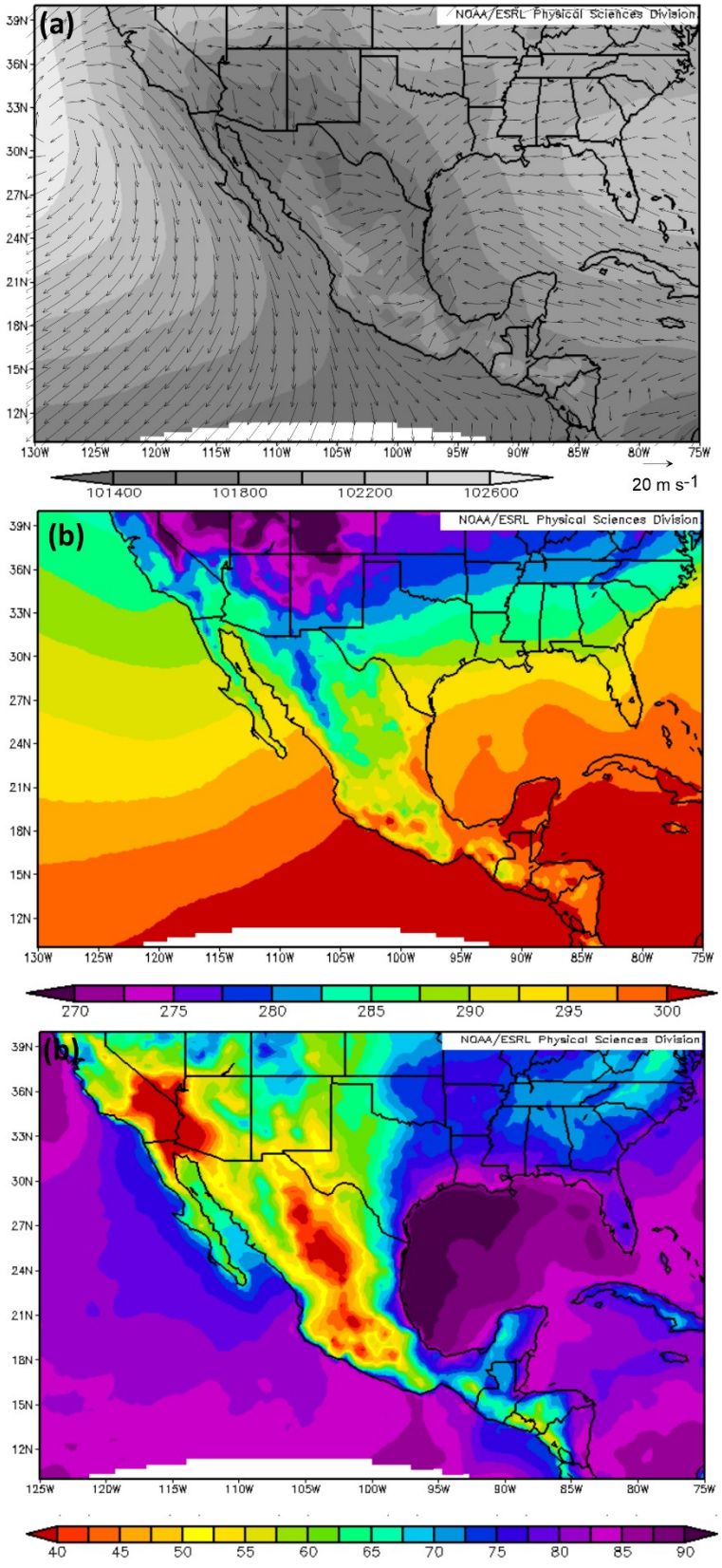
(a)
NOAA/ESRL Physical Sciences Division
39N
36N
33N
30N
27N
24N
21N
18N
15N
12N
130W
125W
120W
115W
110W
105W
100W
95W
90W
85W
80W
75W
101400
101800
102200
102600
20 m s-1
(b)
NOAA/ESRL Physical Sciences Division
270
275
280
285
290
295
300
(b)
NOAA/ESRL Physical Sciences Division
40
45
50
55
60
65
70
75
80
85
90

Figure 5

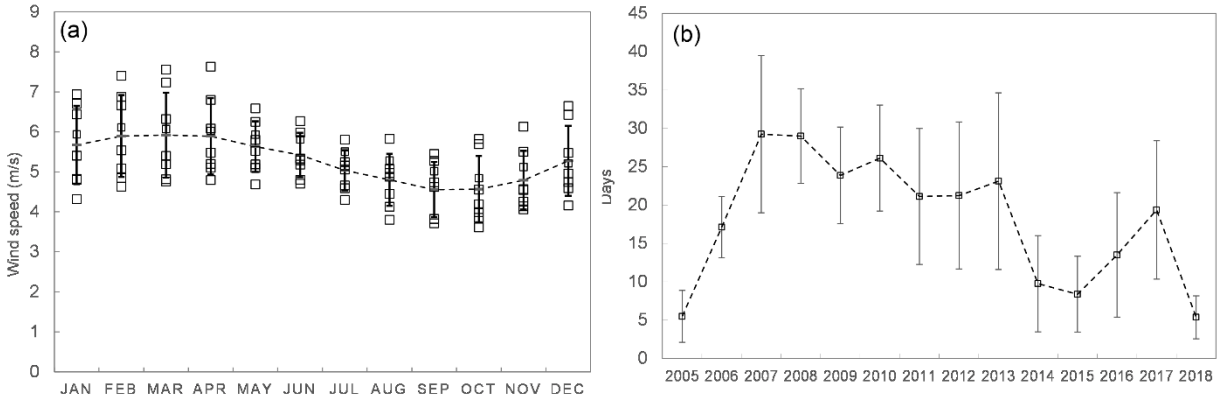

Figure 6

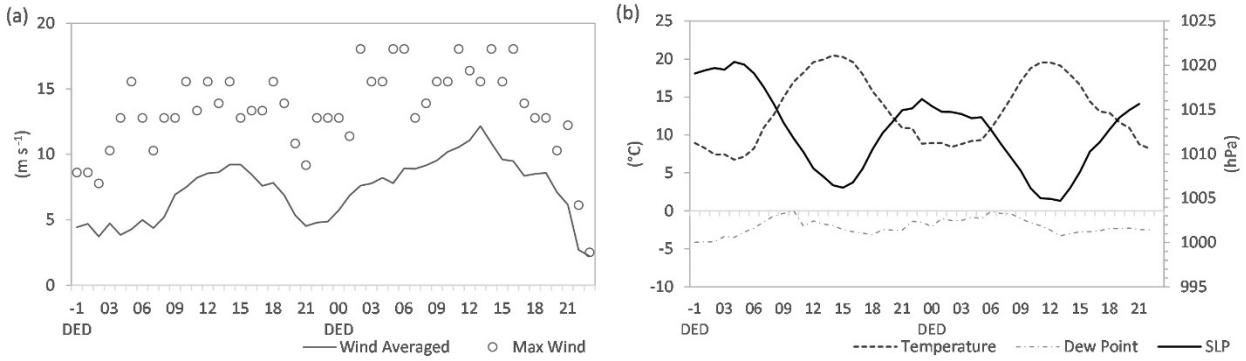

Figure 7

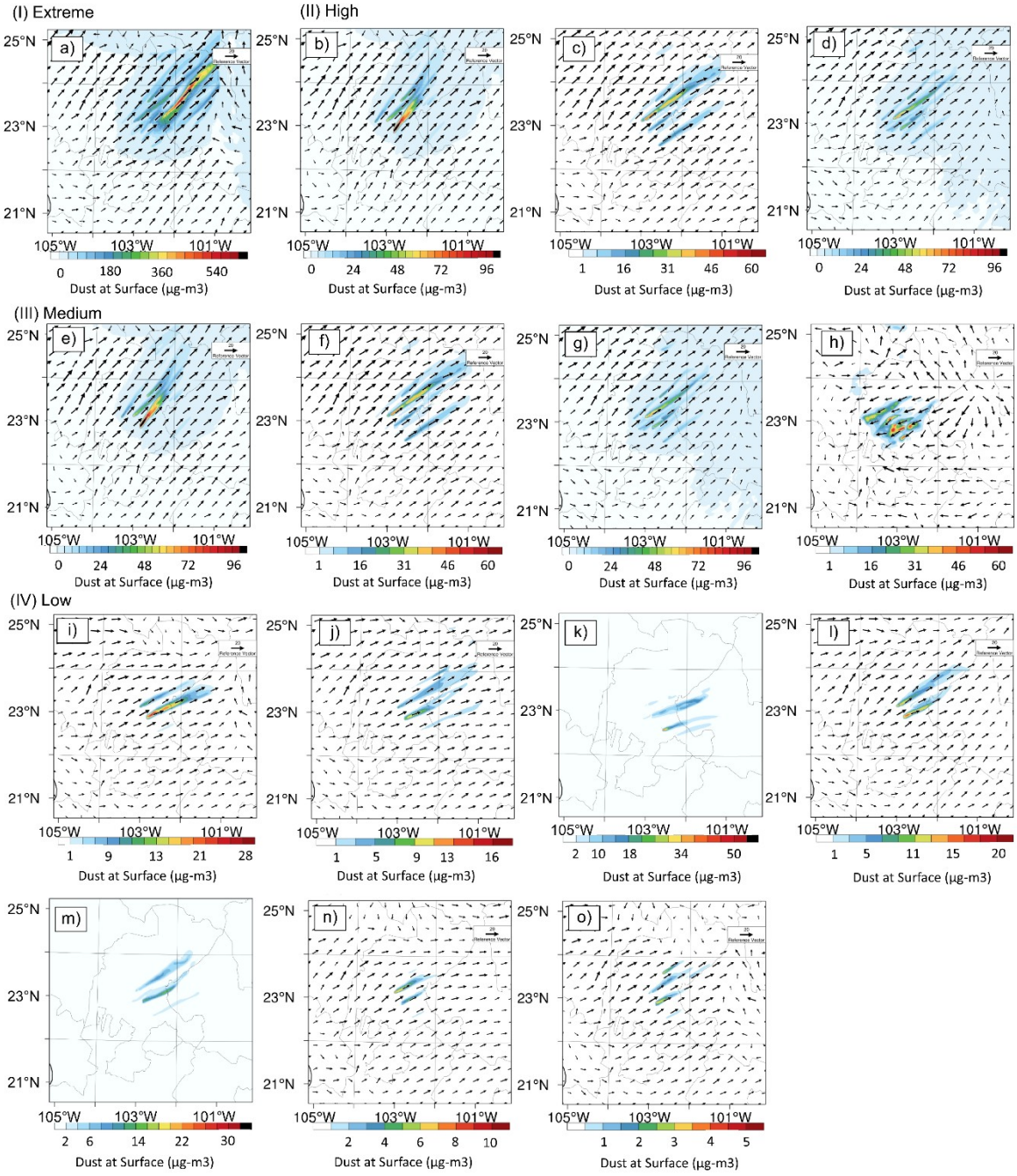
(I) Extreme
(II) High
(III) Medium
(IV) Low
a)
b)
c)
d)
e)
f)
g)
h)
i)
j)
k)
l)
m)
n)
o)
25°N
23°N
21°N
105°W
103°W
101°W
0 180 360 540
0 24 48 72 96
1 16 31 46 60
0 24 48 72 96
1 16 31 46 60
0 24 48 72 96
1 16 31 46 60
1 9 13 21 28
1 5 9 13 16
2 10 18 34 50
1 5 11 15 20
2 6 14 22 30
2 4 6 8 10
1 2 3 4 5
Dust at Surface (µg-m3)

Figure 8

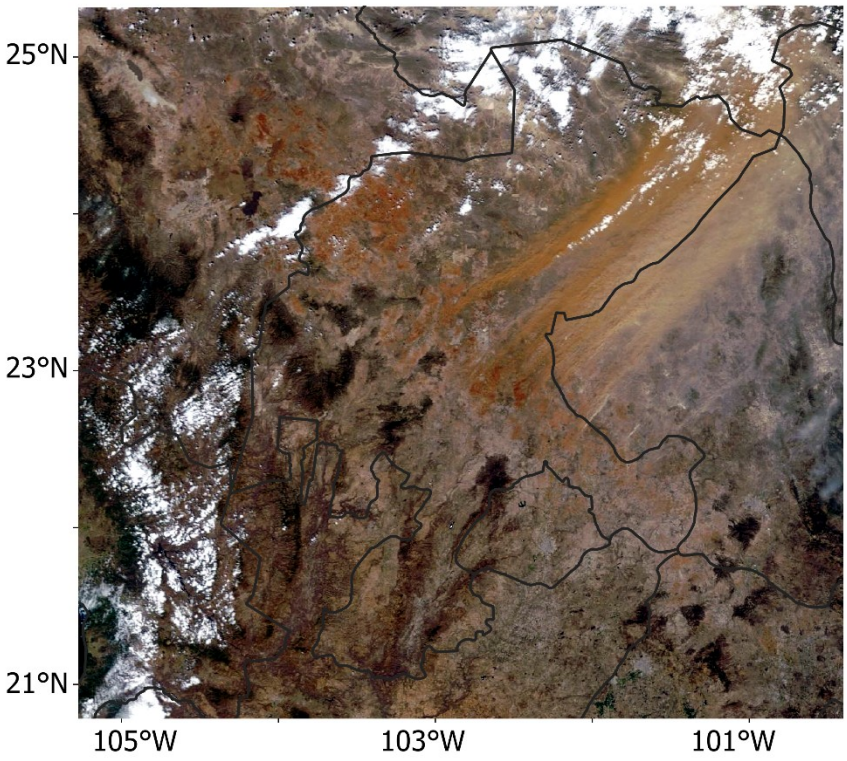

Figure 9

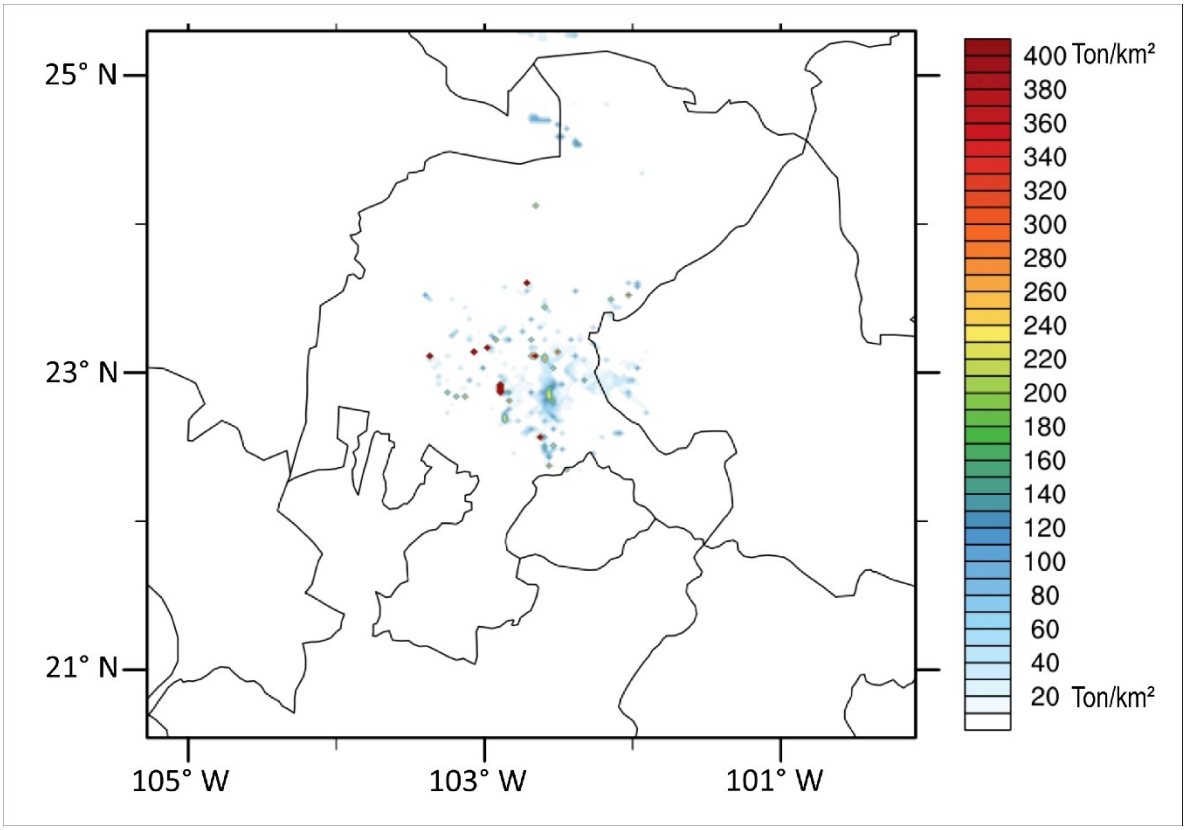
25° N
23° N
21° N
105° W
103° W
101° W
400 Ton/km²
380
360
340
320
300
280
260
240
220
200
180
160
140
120
100
80
60
40
20 Ton/km²

Figure Captions

Figure 1. a) Location map of the study area, dotted lines indicate the simulated area in WRF-Chem D1: domain one, D2: domain two and b) satellite image of a zoom area, red dots indicate the localization where the soil samples were taken, and numbers correspond to weather station: 1) Ábrego, 2) COBAEZ, 3) Emancipación, 4) Las Arcinas, 5) Mesa de Fuentes, 6) Rancho Grande, 7) Santa Rita, 8) U.A. Agronomía, and 9) ZCL International Airport.

Figure 2. Particle size from eight soil samples in the study area.

Figure 3. Composite chart for all dust event days (DED) at 700 mb geopotential height (m) from NCEP/NCAR reanalysis. The left column corresponds to composite mean for (a) The previous day of the event (-1 DED), (b) For the event date, and (c) the following day (+1 DED). In the right column are displayed the anomalies for (d) the previous day of the event (-1 DED), (e) for the event date, and (f) the following day (+1 DED).

Figure 4 Composite of the 15 events just for DED for, a) Composite SLP and wind vectors, b) surface temperature and c) relative humidity.

Figure 5 a) Annual monthly Averaged wind speed for the eight weather stations, and b) Number of the days exceeding the wind speed umbral (>9 m/s).

Figure 6. Average hourly data for the 15 DED's at the center of the domain at Zacatecas International Airport (ZCL), (a) Average hourly wind and maximum wind graphs, and (b) Sea level pressure (SLP), temperatures and Dew point. The data are shown for a previous day (-1 DED).

Figure 7. WRF-Chem data from dust storm events groups. a) The group I represent the extreme case of February 3, 2011. Group II of High intensity of cases b) December 29,

2006, c) January 31, 2007, and d) April 11, 2009. Group III of the medium intensity of cases e) December 1, 2009, f) December 27, 2015, g) March 8, 2016, and h) April 10, 2018. Group IV of Low intensity of cases i) February 14, 2007, j) February 16, 2008, k) March 10, 2010, l) March 20, 2012, m) February 21, 2013, n) February 14, 2017 and o) December 7, 2017.

Figure 8. Reddish dust storm in the study area. Moderate Resolution Imaging Spectroradiometer (MODIS) image, acquired by NASAs Aqua satellite on March 18, 2008.

Figure 9. Estimation of total potential soil loss in 50 years by wind erosion effect. The areas correspond to the model WRF-Chem grids considered as dust area sources.